Applied Catalysis B: Environmental 203 (2017) 654–662

Contents lists available at ScienceDirect

Applied Catalysis B: Environmental

journal homepage: www.elsevier.com/locate/apcatb

Electrochemical and *in situ* FTIR study of the ethanol oxidation reaction on PtMo/C nanomaterials in alkaline media

W.J. Pech-Rodríguez [a], D. González-Quijano [a], G. Vargas-Gutiérrez [a], C. Morais [b], T.W. Napporn [b], F.J. Rodríguez-Varela [a,*]

[a] Cinvestav Unidad Saltillo, Av. Industria Metalúrgica 1062, Parque Industrial Ramos Arizpe, Ramos Arizpe, Coahuila, C.P. 25900, Mexico
[b] Université de Poitiers, UMR CNRS 7285, « Equipe SAMCat », 4, rue Michel Brunet, B27, TSA 51106, 86073 Poitiers Cedex 09, France

ARTICLE INFO

Article history:
Received 17 June 2016
Received in revised form 12 October 2016
Accepted 20 October 2016
Available online 26 October 2016

Keywords:
Ethanol oxidation reaction
Alkaline media
PtMo/C alloys
CO stripping
In situ FTIR analysis

ABSTRACT

In this work, the catalytic activity of PtMo/C catalysts for the Ethanol Oxidation Reaction (EOR) in 0.5 mol L^{-1} KOH electrolyte was evaluated by electrochemical and *in situ* Fourier Transform Infrared Spectroscopy (FTIR) measurements. The alloys having 1:1, 2:1 and 3:1 Pt:Mo atomic ratios were synthesized by the formic acid method. X-ray diffraction analyses (XRD) showed the crystalline features of the catalysts, with crystallite sizes between 2.5 and 3.2 nm. Cyclic voltammograms (CVs) indicated the alloys mass catalytic activity in the order: $Pt_1Mo_1/C > Pt_3Mo_1/C > Pt_2Mo_1/C$, in all cases higher that Pt/C. For specific catalytic activity, the performance was in the order $Pt_3Mo_1/C > Pt_1Mo_1/C$–Pt/C > Pt_2Mo_1/C. Two CO-like species namely CO^{I}_{ads} and CO^{II}_{ads} were evidenced from CO-stripping measurements on the alloys. *In situ* FTIR characterization showed that the alloys promote the oxidation of ethanol in the alkaline media mainly through a 4 electrons transfer route. CO_2 was produced probably from the break-up of the C—C bond and the oxidation of C1 species. Pt_3Mo_1/C produced more CO^{I}_{ads}, followed by Pt_1Mo_1/C, oxidizing carbon monoxide more easily. These two alloys also had a higher CO_2/CH_3CHO ratio, due to a high efficiency for oxidizing C2 and C1 species to CO_2. Such capabilities promoted a higher catalytic activity of Pt_1Mo_1/C and Pt_3Mo_1/C for the EOR, related to the other catalysts.

1. Introduction

Over the last decades, the Direct Alcohol Fuel Cells (DAFCs) have been widely investigated as power sources for stationary and portable applications. These electrochemical devices present energetic advantages such as simple fuel handling, low operating temperature, high energy conversion efficiency and reduced environmental impact [1–5]. Among the different liquid fuels proposed for DAFCs, ethanol is particularly interesting because of its relevant energy density and also its large production from agricultural raw materials and biomass [6,7].

For several decades, the research on DAFCs focused on the use of acid polymer electrolytes [8]. Nevertheless, the recent advances in the development of chemically stable alkaline polymer electrolytes have prompted an increased interest in Alkaline Direct Alcohol Fuel Cells (A-DAFCs) [9,10]. Having the advantage of being devices with a less corrosive environment than that found in their acid counterparts, thus ensuring a longer life-cycle, A-DAFCs are rapidly becoming the subject of study and development worldwide [11–15]. Moreover, A-DAFCs present facile anode and cathode kinetics, compared to acid fuel cells [16–18].

Besides that, it is acknowledged that even in the alkaline media, the complete oxidation of ethanol into CO_2 proceeds through a complex reaction mechanism that involves dissociative adsorption of the molecule, C—C bond cleavage and dehydrogenation. Consequently, it is observed the formation of reaction intermediates that in turn are poison for Pt-alone anode catalysts [19–24]. Nonetheless, it has been reported that at high pH values, the C—C bond breakage, *i.e.*, the so called C1-pathway, is more facile than its acid counterpart [25]. Further reactions induced after the C—C cleavage at ethanol or acetaldehyde, such as the oxidation of $CH_{x,ads}$ and CO_{ads} species leading to CO_2, proceed at more low potentials in alkaline media [25,26]. On the other hand, in the C2-pathway (*i.e.*, no C—C breakage of the ethanol molecule), the rate of acetaldehyde oxidation to acetate increases at high pH [25]. According to Koper et al., the formation of acetaldehyde leads to an increase of the current density during the EOR in alkaline electrolyte [25].

* Corresponding author.
E-mail address: javier.varela@cinvestav.edu.mx (F.J. Rodríguez-Varela).

http://dx.doi.org/10.1016/j.apcatb.2016.10.058
0926-3373/

In spite of that, it is well known also that due to the multi-step reaction mechanism, plurimetallic Pt-based anodes are needed, in order to enhance the tolerance to intermediate species and increase the catalytic activity for the EOR [21,22]. Zhao and co-workers have demonstrated that Pt-Rh/C anodes activate the EOR in KOH solution, improving the C—C bond cleavage and accelerating the oxidation of CO_{ads} species to CO_2, leading to an increase of the catalytic activity compared to Pt/C [21]. The report by Assumpção and co-workers has showed that PtAu/C alloys have a higher catalytic activity than Pt/C for the EOR due to an extension of the Pt lattice parameter, promoting as well the C—C bond breaking [22]. Moreover, Zhu and co-workers have developed hollow Au/Pt core-shell nanostructures, with enhanced catalytic activity and stability for the EOR, in part due to a higher Pt utilization factor at the nanoporous materials [27].

On this regard, the study of an element like Mo in PtMo/C alloys for the EOR in alkaline media has been ignored or at least limited. Mo is an oxophilic metal that has been incorporated as co-catalyst for increasing the catalytic activity for the oxidation of alcohols in acid solutions and also for improvement of the tolerance towards CO, compared with pure Pt anodes [28–32]. It has the advantage of being inexpensive and widely available [19]. In acid electrolyte, PtMo/C is more active than Pt/C for the EOR, even though its performance is lower compared to PtRu/C [32]. In *situ* FTIR and DEMS studies have indicated that the incorporation of Mo to PtRu/C catalysts results in a higher tolerance to CO, leading to acetaldehyde and acetic acid formation [33]. Precisely, the study of the EOR at PtMo/C catalysts in alkaline media and identification of reaction intermediates by *in situ* FTIR is not reported in the literature, to the best of the authorís knowledge.

With the aim to evaluate their catalytic activity for the EOR in alkaline media, this work presents the synthesis of PtMo/C catalysts (Pt:Mo atomic ratios of 1:0, 1:1, 2:1 and 3:1) with formic acid as reducing agent. XRD and EDS analyses were performed in order to assess the crystalline structure and the chemical composition of the materials. Their electrochemical characterization has been studied through cyclic voltammetry (CV), the chronoamperometry and the CO stripping measurements. The identification of reaction intermediates and products was carried out by *in situ* FTIR spectroscopy technique.

2. Experimental

2.1. Materials

Chloroplatinic acid hexahydrate ($H_2PtCl_6{\cdot}6H_2O$), ammonium molybdate tetrahydrate ($(NH_4)_6\ Mo_7O_{24}$), formic acid (HCOOH), ethanol (C_2H_5OH) and potassium hydroxide (KOH) were obtained from Sigma-Aldrich. CO and N_2 gases were of UHP grade (Praxair). Vulcan XC-72 from Cabot® was used as the support.

2.2. Physical and chemical characterization

XRD measurements were performed with a Phillips-Xípert diffractometer using CuKα radiation source, in a scan from 10 to 100° (2θ). The data was refined by using the Savitzky-Golay algorithm. The crystallite size was calculated with the Scherrer equation by analyzing the Pt (220) reflection of each sample. The chemical composition was obtained by a Phillips XL30 SEM microscope equipped with an Energy Dispersive X-ray Spectroscopy (EDS) analyzer operating at 20 kV.

2.3. Synthesis of the electrocatalysts

PtMo/C catalysts with metal loading of 20 wt.% were synthesized by simultaneous reduction of chloroplatinic acid and ammonium molybdate in aqueous medium. An appropriate amount of Vulcan was dispersed by ultrasound in 0.1 mol L^{-1} formic acid for 30 min. The mixture was heated at 80 °C under magnetic stirring and the appropriate quantities of Pt and Mo precursors were added drop by drop, maintaining the temperature for 2 h. The solution was allowed to cool down to room temperature and the final products were filtered, washed, and dried. The same procedure was used with chloroplatinic acid alone for preparing the pure 20 wt.% Pt/C catalyst.

2.4. Electrode preparation and electrochemical measurements

The catalytic activity of the electrocatalysts for the EOR was studied in a three electrode cell (from Pine Inst.), using a Voltalab PGZ 301 potentiostat/galvanostat. The counter electrode was a platinum sheet and the reference electrode was an Ag/AgCl electrode. For simplifying the comparison all potentials reported in this paper were referenced to the RHE scale. The working electrode was a thin catalytic film on glassy carbon (5 mm diam) which is inserted in a Teflon support (Pine Inst.). This catalytic layer was prepared by deposition of 10 μL of a catalytic ink composed of 5 mg of catalyst in a mixture of 0.5 mL isopropyl alcohol and 25 μL Nafion®.

CVs were acquired in N_2-saturated 0.5 mol L^{-1} KOH electrolyte in the potential range between 0.05 V to 1.2 V/RHE at a scan rate of 20 mV s^{-1}, based on the geometrical area of the glassy carbon. The electrochemically active surface area

$\left(ECSA_{H_{UPD}}\right)$ of the anodes was calculated from the charge corresponding to the hydrogen desorption, considering a charge of 210 μC cm^{-2} due to the adsorption of a hydrogen monolayer on Pt. Afterwards, the mass and specific catalytic activities for the EOR were evaluated in an electrolyte containing 0.5 mol L^{-1} C_2H_5OH. In the first case, the amount of Pt at each catalysts (from EDS analysis) was considered. In the second case, the real Pt areas, obtained from the hydrogen desorption regions at the CVs, were taken into account. Chronoamperometric tests were performed by polarizing the electrode at 0.66 V/RHE for 20 min in the presence of ethanol. CO-stripping was carried out as follows: at a constant applied potential of 0.26 V/RHE at the working electrode, CO was bubbled for 10 min. Then the electrolyte was saturated with N_2 for 10 min and CVs were recorded at 20 mV s^{-1}. The electrochemically active surface area ($ECSA_{CO}$) of the electrocatalysts was determined by assuming a charge of 420 μC cm^{-2} due to the adsorption of a CO monolayer at the Pt surface [34].

2.5. In situ *FTIR spectroscopy measurements*

In situ FTIR measurements were carried out under external reflections conditions on a Bruker-IFS66 v spectrometer interfaced with the OPUS 5.5 software (Bruker) and modified for beam reflectance at a 65° incident angle and equipped with a liquid N_2-cooled MCT (HgCdTe) detector. In order to avoid vibration bands from air the system is maintained under vacuum. The experiments were carried out in a three electrode spectroelectrochemicall cell equipped with a CaF_2 window on the bottom and connected to a potentiostat Autolab (PGSTAT-30) interfaced with the Nova 1.8 software. A reversible hydrogen electrode and a glassy carbon slab were respectively used as reference and counter electrodes. The working electrode consisted of a glassy carbon disk of 6 mm diameter (0.282 cm^{-2}) that was polished using alumina powder prior to each experiment. The spectra were acquired using the single potential alteration IR reflectance spectroscopy (SPAIRS) method in the range of 0.1–1.2 V *vs* RHE at 50 mV intervals at a scan rate of 1 mV s^{-1}.The spectra resolution was 4 cm^{-1}, and the FTIR spectra were recorded in the 1000 cm^{-1} and 4000 cm^{-1} MIR region. 512 interferograms were co-added and IR spectra were calculated for each potential values as changes in the reflectivity (R) relative to a

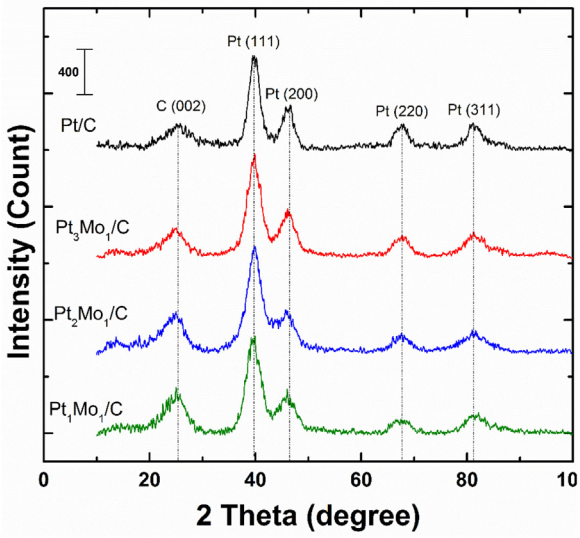

Fig. 1. XRD patterns of the PtMo/C alloys and Pt/C.

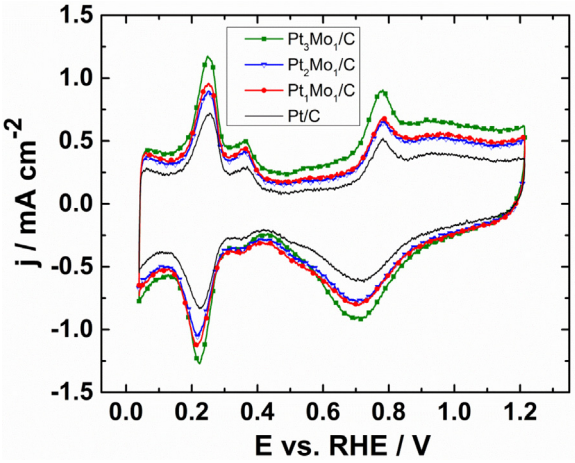

Fig. 2. CVs of Pt-Mo/C and Pt/C catalysts, in N_2-saturated 0.5 M KOH recorded at 20 mV s^{-1} and at room temperature.

reference single-beam spectrum (R_{ref}) taken at 0 V vs RHE as follows: $(\Delta R/R)i = (R_i - R_{ref})/R_{ref}$. According to this definition, negative going (downwards) bands indicated species being generated or an increase in their concentration with respect to the previous potential. Meanwhile, positive going (upward) bands corresponded to a decrease in concentration of the species.

3. Results and discussion

3.1. Physical and chemical characterization

The diffractograms of the PtMo/C alloys and Pt/C are shown in **Error! Reference source not found.** The peak at about $2\theta = 25^\circ$ is attributed to the carbon support. Other peaks at nearly $2\theta = 39$, 46, 67° and 81° are assigned to the Pt reflections (111), (200), (220), and (311), respectively. The planes can be related to the fcc Pt structure. No diffraction patterns of metallic Mo are observed. Moreover the diffraction patterns of the PtMo/C catalysts are slightly shifted to higher 2θ values with respect to Pt/C, suggesting the formation of an alloy, although the formation of amorphous oxides should not be discarded [19,30,35].

Fig. 1.

In order to determine the values of the lattice parameters, the Nelson Riley extrapolation function has been used [36]. The alloys showed a slight lattice contraction compared to the monometallic material (Table 1), indicating the low degree of alloying between Pt and Mo, in good agreement with the characteristics observed for PtMo catalysts in the literature [37,38]. The crystallite size of the nanocatalysts has been calculated from the broadening of the Pt (220) reflection using the Scherrer equation [39]:

$$d = \frac{0.9\lambda_{k\alpha}}{B_{2\theta}\cos\theta} \quad (1)$$

where d is the crystallite size, λ is the X-ray wavelength of the Cu Kα radiation (1.5406 Å), $\beta_{2\theta}$ is the width at half height of the diffraction peak and θ is the angle corresponding to the reflection. The d values are shown in Table 1. There is a decrease in crystallite size of the alloys (ranging from 2.54 to 3.25 nm), related to Pt/C (4.36 nm). There is a correlation between the Mo content and crystallite size: less amount of the alloying element leads to higher values of d.

The EDS results in Table 1 show that the Pt:Mo ratios are close to the expected nominal value, except for Pt_1Mo_1/C which shows some losses of Mo. This behavior can be attributed to the different species that are reduced to lower oxidation states and are highly dependent on pH, resulting in a partial precipitation of the element [40]. Even more, the overall chemical composition of the catalysts approaches that expected (Table 1).

3.2. Electrocatalytic activity for the EOR

Fig. 2 shows the cyclic voltammograms (CVs) of the electrocatalysts in supporting electrolyte KOH 0.5 mol L^{-1}. The so-called hydrogen adsorption regions are observed, with well-defined hydrogen adsorption/desorption peaks, as well as the double layer region and the oxide formation/reduction regions.

The CVs of the mass catalytic activity of the catalysts in the supporting electrolyte in presence of ethanol are shown in Fig. 3(a). During the forward scan the oxidation begins on Pt/C at around 0.185 V vs. RHE and reaches a maximum mass current density of 554.7 mA mg_{Pt}^{-1} at 0.83 V. Pt-Mo nanomaterials showed shifted oxidation peaks, mainly for Pt_1Mo_1/C catalyst, which exhibited the highest mass current density. During the negative sweep, an oxidation peak was observed for all catalysts around 0.70 V vs. RHE. It corresponds to the oxidation of carbonaceous species (either ethanol or reaction intermediates such as CO) that were not completely oxidized during the positive scan [41,42].

From the curves it is possible to observe that the onset potential of the EOR (E_{onset}) considering mass activity is lower at the bimetallic catalysts (see the inset in Fig. 3) compared to Pt/C, with

Table 1
Physicochemical characteristics of the PtMo/C and Pt/C catalysts.

Catalyst	Lattice parameter (nm)	d (nm)	Nominal Pt:Mo ratio (at.%)	Experimental Pt:Mo ratio (at.%)	Chemical composition (wt.%)		
					Pt	Mo	C
Pt/C	0.392	4.36	100:0	100:0	19.96	0	80.04
Pt_3Mo_1/C	0.391	3.25	75:25	74:26	17.50	3.1	79.4
Pt_2Mo_1/C	0.391	2.91	67:33	66:34	14.60	3.77	81.57
Pt_1Mo_1/C	0.390	2.54	50:50	58:42	13.5	4.3	82.2

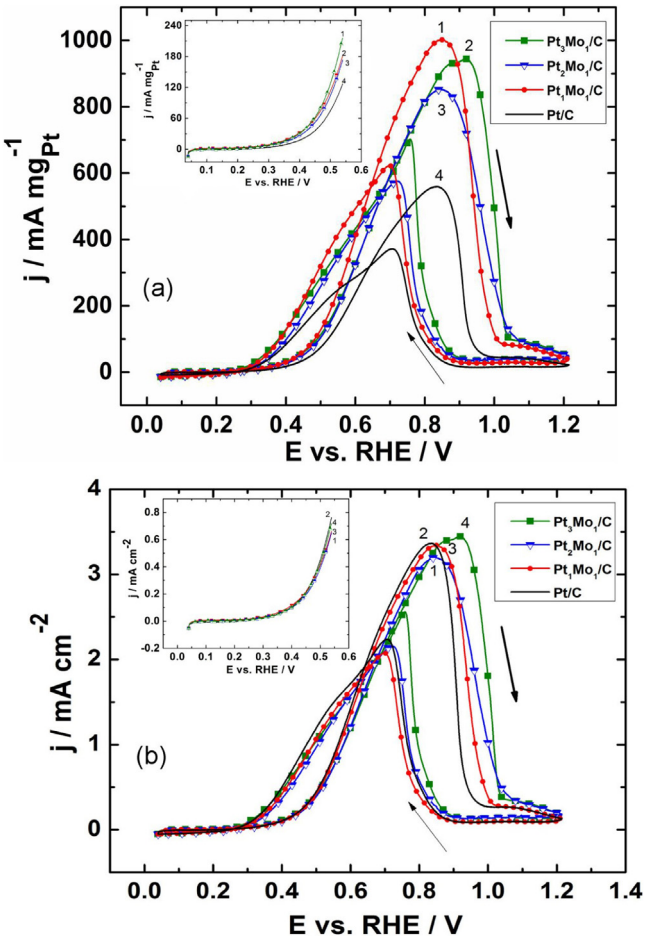

Fig. 3. Ethanol Oxidation Reaction on PtMo/C alloys and Pt/C catalysts: (a) Mass activity; (b) Specific activity. Acquired in N_2-saturated 0.5 mol L^{-1} KOH + 0.5 mol L^{-1} EtOH recorded at 20 mV s^{-1} and at room temperature.

Table 2
Electrochemical parameters of mass catalytic activity for the EOR at the PtMo/C and Pt/C anodes.

Catalysts	E_{onset} (V)	j_f (mA mg_{Pt}^{-1})	j_f/j_b ratio
Pt/C	0.185	554.7	1.50
Pt_3Mo_1/C	0.155	942.0	1.36
Pt_2Mo_1/C	0.175	849.9	1.48
Pt_1Mo_1/C	0.155	1000.0	1.62

Pt_1Mo_1/C and Pt_3Mo_1/C showing the lowest value (Table 2). Also, the alloys delivered higher mass current densities in the forward scan (j_f, Table 2) than Pt/C. Therefore, Pt_1Mo_1/C shows the highest mass current density of 1000.0 mA mg_{Pt}^{-1}. This value of j_f is about 1.8 times that of Pt/C (554.7 mA mg_{Pt}^{-1}). Pt_3Mo_1/C delivers a mass current density of 942.0 mA mg_{Pt}^{-1}, roughly 1.7 higher than Pt/C. Even though attention should be pay to the different experimental conditions, the mass current densities of Pt_1Mo_1/C and Pt_3Mo_1/C are higher than those reported in the literature for similar Pt-based anodes both in alkaline and acid media [43,44].

The alloys show tolerance to the intermediates by delivering low mass current densities in the backward scan (j_b) [45]. On this matter, the j_f/j_b ratio of the PtMo/C anodes is comparable to that of Pt/C (Table 2). Considering the electrochemical parameters extracted from the EOR curves, the mass catalytic activity in alkaline electrolyte decreases in the order: Pt_1Mo_1/C > Pt_3Mo_1/C > Pt_2Mo_1/C > Pt/C.

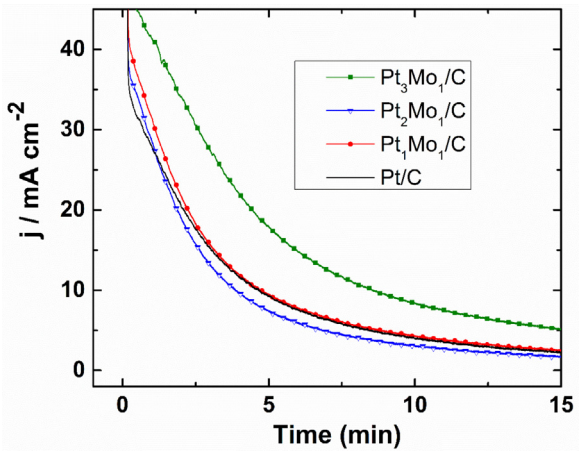

Fig. 4. Chronoamperometric curves of PtMo/C and Pt/C catalysts in 0.5 KOH + 0.5 M EtOH. Applied Potential: 0.66 V/RHE at room temperature.

The CVs of the specific catalytic activity are shown in Fig. 3(b). In terms of specific current density, the highest performance is that of Pt_3Mo_1/C. The Pt_1Mo_1/C alloy shows a performance similar to that of Pt/C, with Pt_2Mo_1/C having slightly lower specific catalytic activity. Meanwhile, the E_{onset} values are similar for the four catalysts (see inset in the Figure).

The enhanced performance of the alloys, particularly Pt_1Mo_1/C and Pt_3Mo_1/C, may be attributed to the bifunctional mechanism due to the incorporation of Mo in the catalysts. Thereby, ethanol molecules will preferentially adsorb on Pt sites, while Mo sites will provide OH species at low potentials (compared to Pt/C) to oxidize the carbonaceous species to CO_2 [40].

In order to study the stability of the electrocatalysts during the EOR, chronoamperometric tests in the 0.5 M KOH + 0.5 M EtOH electrolyte have been performed (Fig. 4). The current density decay indicates the anode poisoning during the ethanol oxidation. The Pt_3Mo_1/C catalyst has a significantly more stable current density after 20 min, followed by Pt_1Mo_1/C. The Pt/C shows an important decay within a few seconds, but after ca. 3 min its performance reaches that of Pt_2Mo_1/C. The behavior of Pt_3Mo_1/C and Pt_1Mo_1/C confirms that their performance for the EOR in the alkaline electrolyte surpasses those of the rest of the catalysts studied in this work.

3.3. CO-stripping measurements

Fig. 5 shows the CO-stripping voltammograms of the different catalysts in supporting electrolyte. The ECSA (in $m^2\ g^{-1}$) of the catalysts has been estimated with the relationship:

$$ECSA_{CO} = \frac{Q_{CO-des}}{Q_{CO} x L_{Pt}} x10^2 \quad (2)$$

where $Q_{CO\text{-}des}$ ($\mu C\ cm^{-2}$) is the electrical charge of CO desorption from the CVs in Fig. 5, Q_{CO} is the theoretical charge required to oxidize a monolayer of CO on Pt (420 $\mu C\ cm^{-2}$), and L_{Pt} is the amount of Pt ($\mu g\ cm^{-2}$) in the electrode.

The determined values of the ECSA are displayed in Table 3. The alloys exhibited higher $ECSA_{CO}$ than Pt/C. Pt_1Mo_1/C and Pt_3Mo_1/C have values of 31.57 and 26.13 $m^2\ g^{-1}$, respectively. Meanwhile Pt_2Mo_1/C and Pt/C show ECSAs of 23.73 and 19.11 $m^2\ g^{-1}$, respectively. The active surface area can also be obtained by integrating the charge associated with the area under the peak in the hydrogen adsorption/desorption region (Fig. 2), using Eq. (3):

$$ECSA_{H_{UPD}} = \frac{Q}{Q_H x L_{Pt}} x10^2 \quad (3)$$

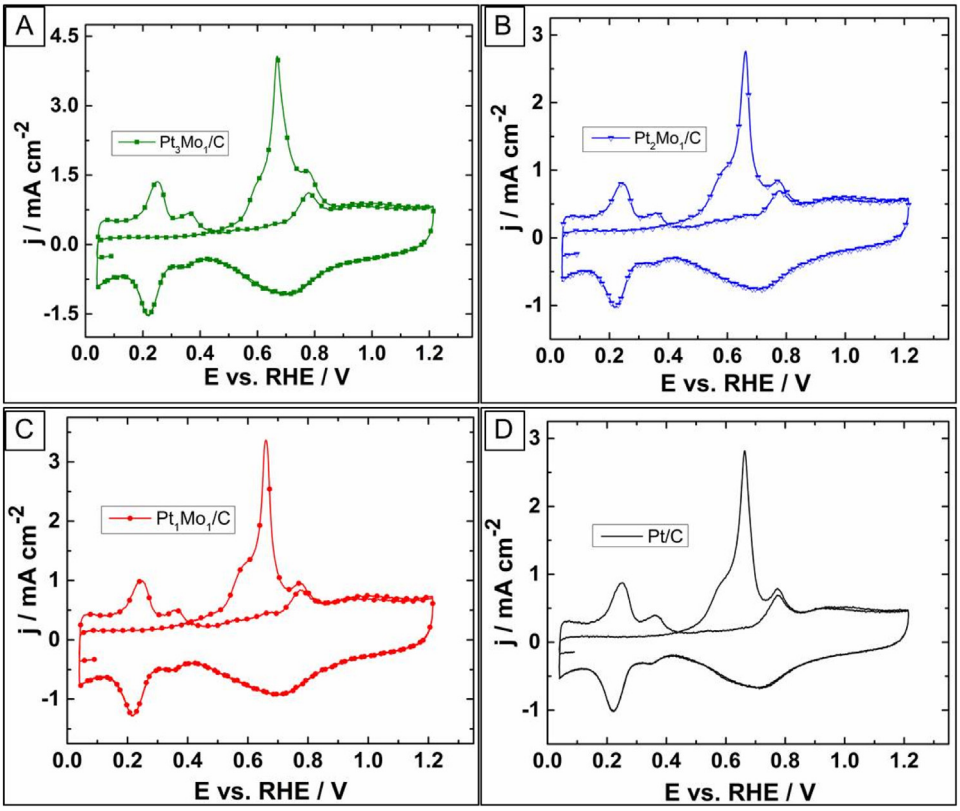

Fig. 5. CO-stripping voltammograms of Pt_3Mo_1/C, Pt_2Mo_1/C, Pt_1Mo_1/C and Pt/C in 0.5 mol L^{-1} KOH recorded at 20 mV s^{-1} and at room temperature. Polarization potential: 260 mV/RHE. CO was bubbled for 10 min, followed by saturation with N_2 for 10 min.

Table 3
ECSA, CSA, Pt utilization and electrical charge from CO-stripping of the catalysts.

Catalyst	$ECSA_{CO}$ ($m^2 g_{Pt}^{-1}$)	$\cdot ECSA_{H_{UPD}} \cdot$ ($m^2 g_{Pt}^{-1}$)	CSA ($m^2 g_{Pt}^{-1}$)	$^1U_{Pt}$ (%)	Q_{CO}^{I} (mC cm^{-2})	Q_{CO}^{II} (mC cm^{-2})	α_1
Pt/C	19.11	16.65	64.30	29.72	4.62	3.53	0.56
Pt_3Mo_1/C	26.13	27.41	86.26	30.20	6.05	3.75	0.61
Pt_2Mo_1/C	23.73	26.60	96.34	24.60	4.69	2.74	0.63
Pt_1Mo_1/C	31.57	30.00	110.38	28.60	5.91	3.22	0.64

[1]Ratio of $ECSA_{CO}$ and CSA

where Q ($\mu C\,cm^{-2}$) corresponds to the integrated charge in the hydrogen adsorption/desorption peak, Q_H is the theoretical charge of 210 $\mu C\,cm^{-2}$ for the adsorption of a monolayer of hydrogen on poly-crystalline Pt, and L_{Pt} is the same as in Eq. (2) [46]. The determined ECSAs from H_{UPD} regions of Pt_1Mo_1/C, Pt_3Mo_1/C, Pt_2Mo_1/C and Pt/C are 30.0, 27.41, 26.60 and 16.65 $m^2\,g^{-1}$, respectively (Table 3). The values obtained confirm those determined by CO-stripping. Higher ECSAs of Pt_1Mo_1/C and Pt_3Mo_1/C are confirmed from the hydrogen adsorption/desorption analysis, suggesting that more active sites are available for the reaction at these catalysts.

The chemical specific surface area (CSA, in $m^2\,g^{-1}$) considers the total surface area of the nanoparticles that may be available for the reaction. It can be calculated based on the assumption that all nanoparticles have a spherical geometry and are not agglomerated with the equation [47]:

$$CSA = \frac{6x10^3}{\rho_{cat} d} \quad (4)$$

where d is the particle diameter determined from XRD analysis and ρ_{cat} is the density of the metals. In the case of platinum its density has been considered as 21.4 g cm^{-3}. For the alloys, it has been taken as $\rho_{cat} = x_{Pt}\rho_{Pt} + y_{Mo}\rho_{Mo}$, where $x_{Pt}\rho_{Pt}$ are the mass fraction and density of platinum, and $y_{Mo}\rho_{Mo}$ are the mass fraction and density of molybdenum (10.2 g cm^{-3}), respectively. The Pt utilization percentage (U_{Pt}) can be estimated from the ratio between ECSA and CSA:

$$U_{Pt} = \frac{ECSA}{CSA} x100 \quad (5)$$

Table 3 shows the parameters obtained for the PtMo/C alloys and Pt/C. As expected because is crystallite size-dependent [47] the CSA from equation (4) follows the particle size trend in Table 1, *i.e.*, a large particle size results in a smaller specific area. Therefore, the CSA of the alloys is higher than that of Pt/C and shows a larger value with higher Mo content. On the other hand, Pt_3Mo_1/C shows the higher Pt atoms utilization (27.92%) among the alloys, a value slightly lower than that of Pt/C (29.72%) (Table 3). These results indicate that reduction of Pt content in PtMo/C alloys has no negative effect in catalytic activity and utilization percentage of the noble metal. Indeed, the high U_{Pt} value of Pt_3Mo_1/C has a positive effect on its catalytic activity towards the EOR, in good agreement with reference [27].

The baseline corrected CO oxidation voltammograms are presented in Fig. 6. A pre-peak of CO oxidation was observed at ~0.6 *vs.* RHE. The current density of the oxidation reaction is higher for Pt_3Mo_1/C, followed by Pt_1Mo_1/C, Pt_2Mo_1/C and Pt/C. The samples exhibit a broad peak, indicating two CO types of CO_{ads} on the surface

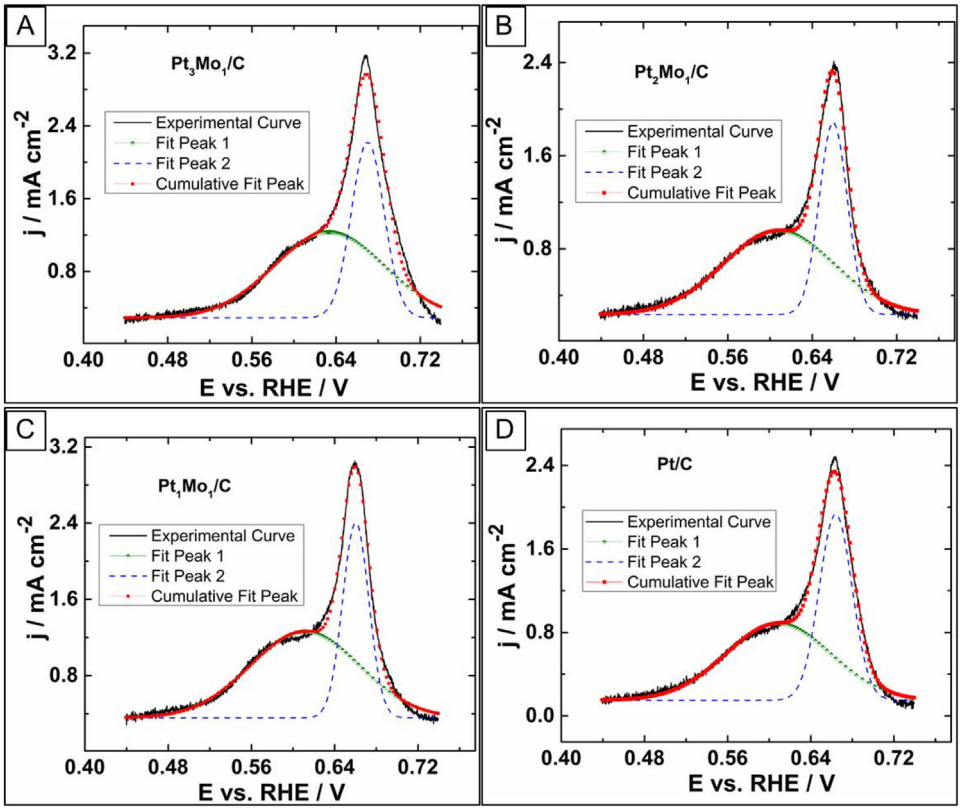

Fig. 6. Baseline-corrected CO oxidation region deconvoluted using a Gaussian distribution.

with different adsorption energies. The area under the curves has been analyzed by deconvoluting the baseline-corrected CO voltammograms using a Gaussian distribution, with an R^2 factor greater than 0.99. Fig. 6 shows the deconvolutions into two peaks that correspond to the two adsorbed species on the Pt sites, named CO^{I}_{ads} and CO^{II}_{ads} [48,49]. The first peak is associated with a weakly bonded CO-like species. Meanwhile, the second peak is ascribed to CO-like species strongly bonded and desorbed at more positive potentials. The charges associated to the desorption of each of the species, Q^{I}_{CO} and Q^{II}_{CO}, have been estimated by integrating the area of the oxidation peaks (Table 3).

The ratio of the surface coverage by each CO_{ads} species can be determined with the relationships [49]:

$$\alpha_1 = \frac{Q^{I}_{CO}}{Q^{I}_{CO} + Q^{II}_{CO}} \quad (6)$$

$$\alpha_2 = \frac{Q^{II}_{CO}}{Q^{I}_{CO} + Q^{II}_{CO}} \quad (7)$$

The values of $_I$ calculated for each catalyst are listed in Table 3. The Pt_3Mo_1/C alloy shows the larger area under the two peaks, with a total charge of 9.80 mC cm^{-2}, followed by Pt_1Mo_1/C, Pt/C and Pt_2Mo_1/C (9.13, 8.15 and 7.43 mC cm^{-2}, respectively). Overall, the PtMo/C alloys have a larger surface coverage of CO^{I}_{ads} and α_1 values than Pt/C. Therefore, the analysis indicates that the alloys can oxidize CO_{ads} more easily than Pt/C, due to the formation of larger amounts of CO^{I}_{ads} at their catalytic surface. Such characteristic has a positive effect on the catalytic activity of the PtMo/C catalysts for the EOR.

3.4. *Analysis by* in situ *FTIR spectroscopy*

Fig. 7 shows the spectra obtained during the EOR for the different studied catalysts. Starting at 400 mV for alloyed compositions, two major bands at 1533 and 1418 cm^{-1} attributed to asymmetric and symmetric C—O bonds stretching vibrations characteristic of acetate ions (CH_3COO-) [50,51] are observed. Moreover, the vibrations at 1418 cm^{-1} show a higher intensity than those at 1533 cm^{-1}, because of an overlapping with the carbonate ion CO_3^{-2} that appears at ~1390 cm^{-1} during the EOR in alkaline media on Pt-based catalysts [52–54]. The presence of carbonate ions may create a physical barrier on the Pt active sites, limiting their ability for ethanol adsorption and its subsequent oxidation [53]. These peaks become more intense as the potential values increase, at the same time that an increase in the consumption of OH^- species occurs as indicated by the bands between 2500 and 3000 and 1700–2000 cm^{-1}. This characteristic also indicates the ethanol consumption according to the ethanol oxidation mechanism proposed elsewhere [55]. The acetate ions vibration bands emerge more clearly on Pt/C at 600 mV, having an intensity that is lower compared to the alloys, particularly the signal at 1533 cm^{-1}.

It is worth mentioning that no CO signals have been detected in the spectra. In previous reports, vibrations due to bridge-bonded CO have been identified at ~1840 cm^{-1} [51]. Still, the formation of CO_{ads} should not be discarded, in view of reports which indicate that its detection in alkaline media is difficult [52]. The EOR in this study may proceed with the formation of low concentrations of CO_{ads}, but its detection has been complicated because of the important concentration of acetate in agreement with the results reported by Shen et al. [52]. Furthermore, the amount of CO_{ads} formed can be more easily oxidized on the alloys as shown from the CO-stripping measurements.

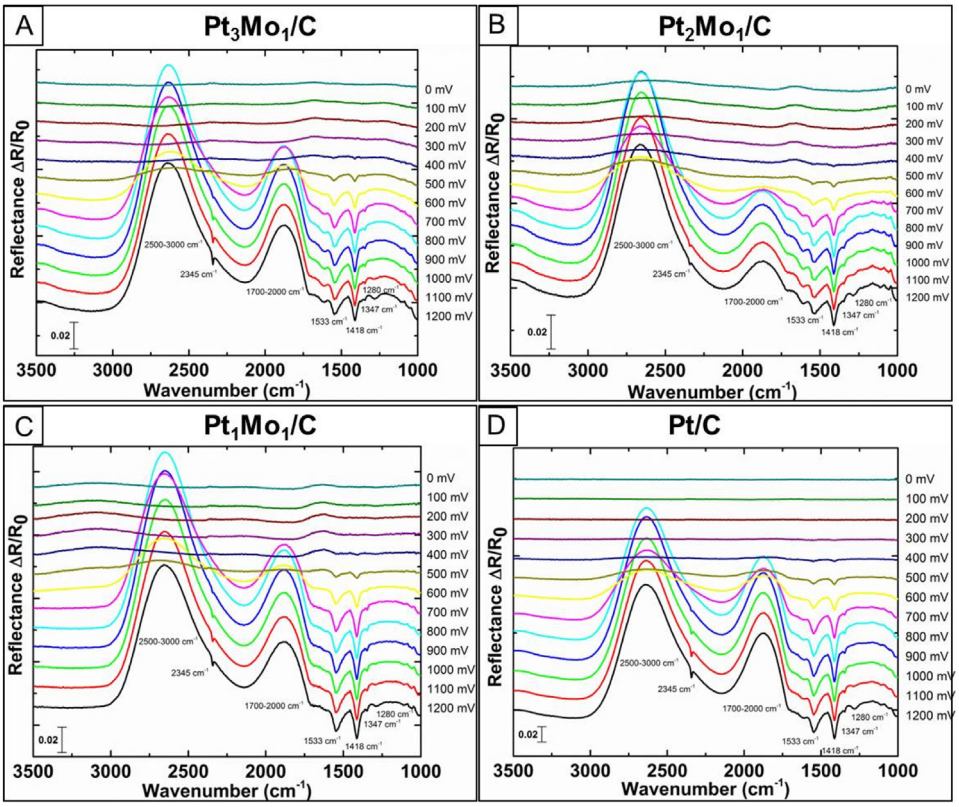

Fig. 7. *In situ* FTIR spectra of the EOR at Pt/C and PtMo/C catalysts. Electrolyte: 0.5 M KOH + 0.5 M EtOH.

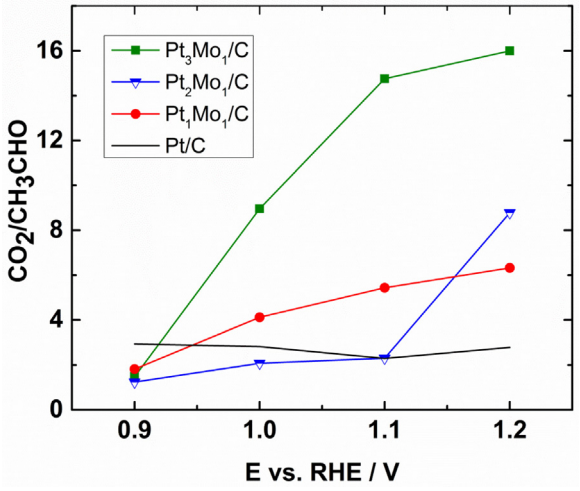

Fig. 8. Ratios of the integrated intensities corresponding to CO_2 (2345 cm^{-1}) and CH_3CHO (1347 cm^{-1}).

The band at 1347 cm^{-1} may be attributed to acetaldehyde (CH_3CHO). Such identification is made according to the report by Neto et al., where the band in the 1390–1290 cm^{-1} region was deconvoluted, showing the presence of a signal around 1343 cm^{-1} due to CH_3CHO [56]. At 900 mV and higher, a peak at 2345 cm^{-1} associated with the CO_2 symmetric stretching vibrations is observed [57]. This signal is more intense at Pt_3Mo_1/C and Pt_1Mo_1/C. The peak at 1280 cm^{-1} which also becomes more intense at higher potentials is attributed to the formation of acetic acid (CH_3COOH) [58,59] confirming the acidification of the electrolyte nearby the electrode.

Table 4
P_2/P_1 integrated band intensity ratios at the catalysts.

	Ratio at different potentials (in mV)				
Catalysts	600	700	800	900	1000
Pt/C	1.60	1.76	1.86	1.87	1.87
Pt_3Mo_1/C	1.18	1.37	1.47	1.42	1.42
Pt_2Mo_1/C	1.61	1.77	2.03	1.96	2.02
Pt_1Mo_1/C	1.12	1.29	1.39	1.35	1.35

Fig. 8 shows the ratios of the integrated intensities of CO_2 and CH_3CHO, from 900 to 1200 mV. The Pt_3Mo_1/C has higher values because significant amounts of CO_2 are formed probably from CO_{ads}. Moreover, it should be noted that CO_2 may be produced *via* acetaldehyde adsorption [32]. This alloy easily promotes the oxidation of carbon monoxide mainly through the CO^l_{ads} species as discussed earlier and thus is less affected by its presence. This is one of the factors of its higher catalytic activity for the EOR. The behavior of Pt_3Mo_1/C is followed by Pt_1Mo_1/C and Pt_2Mo_1/C. At 900 mV, Pt/C shows a higher ratio, but then it tends to decrease suggesting a lower efficiency to oxidize CO_{ads} to CO_2.

In order to compare the rate of CO_3^{-2} formation on the catalysts, the integrated band intensity ratios between the peaks at 1418 cm^{-1} (P_2) and 1553 cm^{-1} (P_1) have been determined [54]. Table 4 shows the P_2/P_1 ratios at different potentials. Pt_1Mo_1/C and Pt_3Mo_1/C show lower values at all potentials evaluated, indicating that the EOR at these catalysts proceeds avoiding high rates of C—C bond cleavage thus limiting the formation of carbonate ions [60]. Meanwhile, Pt_2Mo_1/C and Pt/C have higher ratios, confirming that these two materials form more absorbed carbonaceous species that have a detrimental effect on their catalytic activity.

The evolution of the formation of acetaldehyde, CO_2, carbonate ions and acetate at several potentials are shown in Fig. 9. For this plot, the intensity of each band has been normalized with respect to the intensity of the respective species at 1.0 V. Pt_3Mo_1/C and

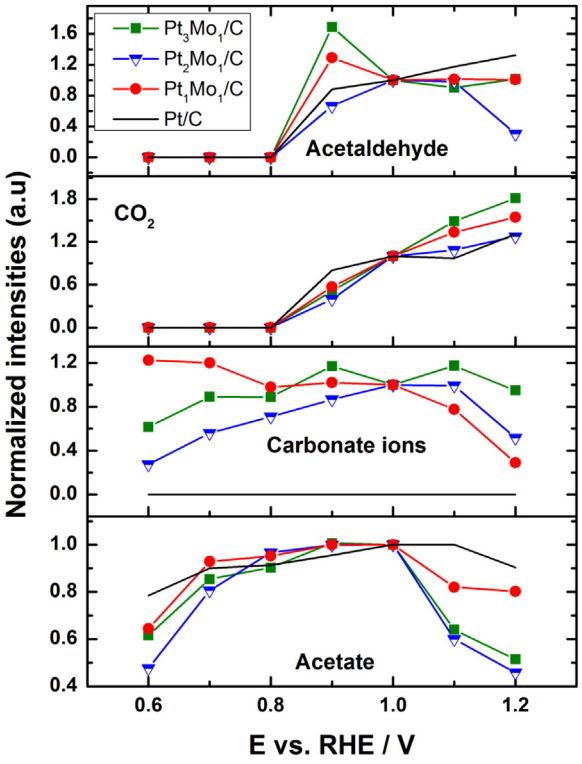

Fig. 9. Evolution of acetaldehyde, CO2, carbonate ions and acetate in the 0.6–1.2 V potential interval, at the PtMo/C and Pt/C catalysts.

Pt_1Mo_1/C form more acetaldehyde in the 0.8–1 V *vs.* RHE region. Starting from 1 V, these two alloys produce more CO_2. The tendency is similar in the case of the carbonate ion: its production if higher in the case of Pt_3Mo_1/C and Pt_1Mo_1/C over 0.8–1 V vs. RHE. Meanwhile, for the acetate there is no clear tendency over the potential range evaluated. Nevertheless, the evolution of the several species in Fig. 9 indicate that Pt_3Mo_1/C and Pt_1Mo_1/C can handle more easily some of the intermediate species and at higher potentials form more CO_2.

It is well known that the EOR on Pt-based catalysts may proceed following the C_1 pathway, where C—C carbon bonds are broken. In this mechanism, ethanol molecules form CO_{ads} which is further oxidized to CO_2. On the other hand, in the C_2 pathway, C—C carbon bond cleavage is avoided resulting in the formation of CH_3CHO and CH_3COOH, which are also oxidized to CO_2. Some adsorbed CH_3COOH may also remain in the catalytic Pt surface without being oxidized [32]. The reactions are, as reported by dos Santos et al. [50]:

$$CH_3CH_2OH + 2OH^- \rightarrow CH_3CHO + 2H_2O + 2e^- \quad (8)$$

$$CH_3CH_2OH + 4OH^- \rightarrow CH_3COOH + 3H_2O + 4e^- \quad (9)$$

$$CH_3CH_2OH + 12OH^- \rightarrow 2CO_2 + 9H_2O + 12e^- \quad (10)$$

The results shown in this work demonstrate that the catalysts promote the oxidation of ethanol in the alkaline electrolyte, mainly through the C2-pathway of $4e^-$ transfer (reaction 9). Moreover, CO_2 is produced probably from a combination of oxidation of C2 and to a lesser extent C1 species [32]. Even though CO_{ads} has not been detected in the spectra of Fig. 9, its contribution to the CO_2 production should not be discarded. Even more, the slight extension of the lattice parameter of the alloys related to Pt/C may have a limited effect on the C—C bond cleavage, which may be one of the reasons of the C2-pathway. In view of these results, the Pt_3Mo_1/C and Pt_1Mo_1/C show a higher catalytic activity for the EOR because of their higher CO_2/CH_3CHO ratio and less production of CO_3^{-2}.

4. Conclusions

PtMo/C electrocatalysts were synthesized using the formic acid method. The XRD patterns showed crystalline nanostructured materials with particle size between 2.54 and 3.25 nm.

The evaluation of catalytic activity of the catalysts towards the EOR demonstrated a higher performance of the PtMo/C alloys, in the alkaline media, compared to Pt/C. Among them, Pt_1Mo_1/C and Pt_3Mo_1/C are the best compositions, showing the highest catalytic activity. For mass catalytic activity, the Pt_1Mo_1/C and Pt_3Mo_1/C anodes delivered a j_f 1.8 and 1.7 higher than Pt/C, respectively, with an onset potential 30 mV more negative.

From CO-stripping measurements it was found that the catalysts exhibited broad pre-peaks, which suggest that two different CO species are oxidized. Indeed, on the alloys, large amounts of CO^I_{ads} are oxidized reducing the poisoning effect by carbon monoxide.

The *in situ* FTIR characterizations showed that the alloys promote the oxidation of ethanol in the alkaline media mostly through a $4e^-$ route. CO_2 was also produced probably from a combination of oxidation of C2 and C1 ($12e^-$ route) species. Even though CO_{ads} was not detected, its contribution to the CO_2 production should not be discarded. In view of these results, it can be concluded that Pt_1Mo_1/C and Pt_3Mo_1/C showed the highest catalytic activity for the EOR because of a combination of issues: i) they form preferentially CO^I_{ads} species, oxidizing carbon monoxide more easily and at lower potentials compared to the other catalysts; ii) they have higher CO_2/CH_3CHO ratio, suggesting a higher efficiency of the alloys to oxidize C2 and C1 species to CO_2; iii) they produce relatively low amounts of CO_3^{-2}.

Acknowledgements

This work was financially supported by the Mexican National Council for Science and Technology (CONACYT) through grants 252079, 241526 and 252003. We thank CONACYT for doctoral scholarships and support through the *Programa de Becas Mixtas* provided to WJPR and DGQ.

References

[1] E. Antolini, Carbon supports for low-temperature fuel cell catalysts, Appl. Catal. B 88 (2009) 1–24.
[2] J.R.C. Salgado, E. Antolini, E.R. Gonzalez, Preparation of Pt-Co/C electrocatalysts by reduction with borohydride in acid and alkaline media: the effect on the performance of the catalyst, J. Power Sources 138 (2004) 56–60.
[3] Y.-Y. Chu, Z.-B. Wang, D.-M. Gu, G.-P. Yin, Performance of Pt/C catalysts prepared by microwave-assisted polyol process for methanol electrooxidation, J. Power Sources 195 (2010) 1799–1804.
[4] S.M.S. Kumar, N. Hidyatai, J.S. Herrero, S. Irusta, K. Scott, Efficient tuning of the Pt nano-particle mono-dispersion on Vulcan XC-72R by selective pre-treatment and electrochemical evaluation of hydrogen oxidation and oxygen reduction reactions, Int. J. Hydrogen Energy 36 (2011) 5453–5465.
[5] S. Sen Gupta, J. Datta, An investigation into the electro-oxidation of ethanol and 2-propanol for application in direct alcohol fuel cells (DAFCs), J. Chem. Sci. 117 (2005) 337–344.
[6] H. Pramanik, A.A. Wragg, S. Basu, Studies of some operating parameters and cyclic voltammetry for a direct ethanol fuel cell, J. Appl. Electrochem. 38 (2008) 1321–1328.
[7] S. Song, P. Tsiakaras, Recent progress in direct ethanol proton exchange membrane fuel cells (DE-PEMFCs), Appl. Catal. B 63 (2006) 187–193.
[8] M.L. Perry, T.F. Fuller, A historical perspective of fuel cell technology in the 20th century, J. Electrochem. Soc. 149 (2002) S59–S67.
[9] G. Merle, M. Wessling, K. Nijmeijer, Anion exchange membranes for alkaline fuel cells: a review, J. Membr. Sci. 377 (2011) 1–35.
[10] B.Y.S. Lin, D.W. Kirk, S.J. Thorpe, Performance of alkaline fuel cells: a possible future energy system? J. Power Sources 161 (2006) 474–483.
[11] E. Antolini, E.R. Gonzalez, Alkaline direct alcohol fuel cells, J. Power Sources 195 (2010) 3431–3450.
[12] Y.S. Li, T.S. Zhao, A high-performance integrated electrode for anion-exchange membrane direct ethanol fuel cells, Int. J. Hydrogen Energy 36 (2011) 7707–7713.
[13] E.H. Yu, K. Scott, Development of direct methanol alkaline fuel cells using anion exchange membranes, J. Power Sources 137 (2004) 248–256.

[14] L. An, T.S. Zhao, L. Zeng, X.H. Yan, Performance of an alkaline direct ethanol fuel cell with hydrogen peroxide as oxidant, Int. J. Hydrogen Energy 39 (2014) 2320–2324.
[15] L. An, T.S. Zhao, An alkaline direct ethanol fuel cell with a cation exchange membrane, Energy. Environ. Sci. 4 (2011) 2213–2217.
[16] J.R. Varcoe, R.C.T. Slade, G.L. Wright, Y. Chen, Steady-State dc and impedance investigations of H_2/O_2 alkaline membrane fuel cells with commercial Pt/C Ag/C, and Au/C cathodes, J. Phys. Chem. B 110 (2006) 21041–21049.
[17] J.R. Varcoe, R.C.T. Slade, Prospects for alkaline anion-exchange membranes in low temperature fuel cells, Fuel Cells 5 (2005) 187–200.
[18] H. Takahashi, M. Sagihara, M. Taguchi, Electrochemically reduced Pt oxide thin film as a highly active electrocatalyst for direct ethanol alkaline fuel cell, Int. J. Hydrogen Energy 39 (2014) 18424–18432.
[19] Z.-B. Wang, G.-P. Yin, Y.-G. Lin, Synthesis and characterization of PtRuMo/C nanoparticle electrocatalyst for direct ethanol fuel cell, J. Power Sources 170 (2007) 242–250.
[20] Y. Wang, S. Song, G. Andreadis, H. Liu, P. Tsiakaras, Understanding the electrocatalytic activity of PtxSny in direct ethanol fuel cells, J. Power Sources 196 (2011) 4980–4986.
[21] S.Y. Shen, T.S. Zhao, J.B. Xu, Carbon supported PtRh catalysts for ethanol oxidation in alkaline direct ethanol fuel cell, Int. J. Hydrogen Energy 35 (2010) 12911–12917.
[22] S.G. da Silva, J.C.M. Silva, G.S. Buzzo, R.F.B. De Souza, E.V. Spinacé, A.O. Neto, M.H.M.T. Assumpção, Electrochemical and fuel cell evaluation of PtAu/C electrocatalysts for ethanol electro-oxidation in alkaline media, Int. J. Hydrogen Energy 39 (2014) 10121–10127.
[23] Z.X. Liang, T.S. Zhao, J.B. Xu, L.D. Zhu, Mechanism study of the ethanol oxidation reaction on palladium in alkaline media, Electrochim. Acta 54 (2009) 2203–2208.
[24] S. Sun, Z. Jusys, R.J. Behm, Electrooxidation of ethanol on Pt-based and Pd-based catalysts in alkaline electrolyte under fuel cell relevant reaction and transport conditions, J. Power Sources 231 (2013) 122–133.
[25] S.E.F. Lai, F.T.Z. Öztürk, V.C. van Rees Vellinga, J. Koning, P. Rodriguez, M.T.M. Koper, Effects of electrolyte pH and composition on the ethanol electro-oxidation reaction, Catal. Today 154 (2010) 92–104.
[26] S.C.S. Lai, M.T.M. Koper, Ethanol electro-oxidation on platinum in alkaline media, Phys. Chem. Chem. Phys. 11 (2009) 10446–10456.
[27] C. Zhang, A. Zhu, R. Huang, Q. Zhang, Q. Liu, Hollow nanoporous Au/Pt core–shell catalysts with nanochannels and enhanced activities towards electro-oxidation of methanol and ethanol, Int. J. Hydrogen Energy 39 (2014) 8246–8256.
[28] D.M. Dos Anjos, K.B. Kokoh, J.M. Léger, A.R.D. Andrade, P. Olivi, G. Tremiliosi-Filho, Electrocatalytic oxidation of ethanol on Pt?Mo bimetallic electrodes in acid medium, J. Appl. Electrochem. 36 (2006) 1391–1397.
[29] E.I. Santiago, M.S. Batista, E.M. Assaf, E.A. Ticianelli, Mechanism of CO tolerance on molybdenum-Based electrocatalysts for PEMFC, J. Electrochem. Soc. 151 (2004) A944–A949.
[30] E.I. Santiago, G.A. Camara, E.A. Ticianelli, CO tolerance on PtMo/C electrocatalysts prepared by the formic acid method, Electrochim. Acta 48 (2003) 3527–3534.
[31] A.L.N. Pinheiro, A. Oliveira-Neto, E.C. De Souza, J. Perez, V.A. Paganin, E.A. Ticianelli, E.R. Gonzalez, Electrocatalysis on noble metal and noble metal alloys dispersed on high surface area carbon, J. New Mater. Electrochem. Syst. 6 (2003) 1–8.
[32] A. Oliveira Neto, M.J. Giz, J. Perez, E.A. Ticianelli, E.R. Gonzalez, The electro-oxidation of ethanol on pt-Ru and Pt-Mo particles supported on high-surface-area carbon, J. Electrochem. Soc. 149 (2002) A272–A279.
[33] G. García, N. Tsiouvaras, E. Pastor, M.A. Peña, J.L.G. Fierro, M.V. Martínez-Huerta, Ethanol oxidation on PtRuMo/C catalysts: in situ FTIR spectroscopy and DEMS studies, Int. J. Hydrogen Energy 37 (2012) 7131–7140.
[34] A. Pozio, M. De Francesco, A. Cemmi, F. Cardellini, L. Giorgi, Comparison of high surface Pt/C catalysts by cyclic voltammetry, J. Power Sources 105 (2002) 13–19.
[35] S. Chen, F. Ye, W. Lin, Effect of operating conditions on the performance of a direct methanol fuel cell with PtRuMo/CNTs as anode catalyst, Int. J. Hydrogen Energy 35 (2010) 8225–8233.
[36] B.D. Cullity, S.R. Stock, Elements of X-Ray Diffraction, third ed., Prentice Hall, 2001.
[37] S. Ball, A. Hodgkinson, G. Hoogers, S. Maniguet, D. Thompsett, B. Wong, The proton exchange membrane fuel cell performance of a carbon supported PtMo catalyst operating on reformate, Electrochem. Solid State Lett. 5 (2002) A31–A34.
[38] L.C. Ordóñez, P. Roquero, P.J. Sebastian, J. Ramírez, Carbon-supported platinum-molybdenum electro-catalysts for methanol oxidation, Catal. Today 107–108 (2005) 46–52.
[39] Z. Guo, H. Zhu, X. Zhang, F. Wang, Y. Guo, Y. Wei, Microwave-assisted synthesis of high-loading, highly dispersed Pt/carbon aerogel catalyst for direct methanol fuel cell, Bull. Mater. Sci. 34 (2011) 577–581.
[40] N.P. Lebedeva, G.J.M. Janssen, On the preparation and stability of bimetallic PtMo/C anodes for proton-exchange membrane fuel cells, Electrochim. Acta 51 (2005) 29–40.
[41] F. Cheng, X. Dai, H. Wang, S.P. Jiang, M. Zhang, C. Xu, Synergistic effect of Pd–Au bimetallic surfaces in Au-covered Pd nanowires studied for ethanol oxidation, Electrochim. Acta 55 (2010) 2295–2298.
[42] W. Ye, J. Yan, Q. Ye, F. Zhou, Template-free and direct electrochemical deposition of hierarchical dendritic gold microstructures: growth and their multiple applications, J. Phys. Chem. C 114 (2010) 15617–15624.
[43] Liang Ma, Deryn Chu, Rongrong Chen, Comparison of ethanol electro-oxidation on Pt/C and Pd/C catalysts in alkaline media, Int. J. Hydrogen Energy 37 (2012) 11185–11194.
[44] Rongfang Wang, Bangxing Wei, Hui Wang, Shan Ji, Julian Key, Xiangtai Zhang, Ziqiang Lei, An effective electrocatalyst for ethanol oxidation: Pt-modified IrCu alloy nanoparticle, Ionics 17 (2011) 595–601.
[45] A. Dutta, S.S. Mahapatra, J. Datta, High performance PtPdAu nano-catalyst for ethanol oxidation in alkaline media for fuel cell applications, Int. J. Hydrogen Energy 36 (2011) 14898–14906.
[46] S. Yin, P.K. Shen, S. Song, S.P. Jiang, Functionalization of carbon nanotubes by an effective intermittent microwave heating-assisted HF/H_2O_2 treatment for electrocatalyst support of fuel cells, Electrochim. Acta 54 (2009) 6954–6958.
[47] T.S. Almeida, L.M. Palma, P.H. Leonello, C. Morais, K.B. Kokoh, A.R. De Andrade, An optimization study of PtSn/C catalysts applied to direct ethanol fuel cell: effect of the preparation method on the electrocatalytic activity of the catalysts, J. Power Sources 215 (2012) 53–62.
[48] N.M. Marković, B.N. Grgur, C.A. Lucas, P.N. Ross, Electrooxidation of CO and H_2/CO mixtures on Pt(111) in acid solutions, J. Phys. Chem. B 103 (1999) 487–495.
[49] V.A. Sethuraman, B. Lakshmanan, J.W. Weidner, Quantifying desorption and rearrangement rates of carbon monoxide on a PEM fuel cell electrode, Electrochim. Acta 54 (2009) 5492–5499.
[50] A.N. Geraldes, D. Furtunato da Silva, J.C. Martins da Silva, O. Antonio de Sá, E.V. Spinacé, A.O. Neto, M. Coelho dos Santos, Palladium and palladium–tin supported on multi wall carbon nanotubes or carbon for alkaline direct ethanol fuel cell, J. Power Sources 275 (2015) 189–199.
[51] Z.-Y. Zhou, Q. Wang, J.-L. Lin, N. Tian, S.-G. Sun, In situ FTIR spectroscopic studies of electrooxidation of ethanol on Pd electrode in alkaline media, Electrochim. Acta 55 (2010) 7995–7999.
[52] X. Fang, L. Wang, P.K. Shen, G. Cui, C. Bianchini, An in situ Fourier transform infrared spectroelectrochemical study on ethanol electrooxidation on Pd in alkaline solution, J. Power Sources 195 (2010) 1375–1378.
[53] E.H. Fontes, R.M. Piasentin, J.M.S. Ayoub, J.C.M. da Silva, M.H.M.T. Assumpção, E.V. Spinacé, A.O. Neto, R.F.B. de Souza, Electrochemical and in situ ATR-FTIR studies of ethanol electro-oxidation in alkaline medium using PtRh/C electrocatalysts, Mater. Renew. Sustain. Energy 4 (2015) 1–10.
[54] L.Q. Wang, M. Bevilacqua, J. Filippi, P. Fornasiero, M. Innocenti, A. Lavacchi, A. Marchionni, H.A. Miller, F. Vizza, Electrochemical growth of platinum nanostructures for enhanced ethanol oxidation, Appl. Catal. B 165 (2015) 185–191.
[55] Z.-X. Liang, T.S. Zhao, Catalysts for alcohol-Fuelled direct oxidation fuel cells, R. Soc. Chem. (2012).
[56] A.O. Neto, J. Nandenha, M.H.M.T. Assumpção, M. Linardi, E.V. Spinacé, R.F.B. de Souza, In situ spectroscopy studies of ethanol oxidation reaction using a single fuel cell/ATR-FTIR setup, Int. J. Hydrogen Energy 38 (2013) 10585–10591.
[57] F. Vigier, S. Rousseau, C. Coutanceau, J.-M. Leger, C. Lamy, Electrocatalysis for the direct alcohol fuel cell, Top. Catal. 40 (2006) 111–121.
[58] G.A. Camara, T. Iwasita, Parallel pathways of ethanol oxidation: the effect of ethanol concentration, J. Electroanal. Chem. 578 (2005) 315–321.
[59] L. Rao, Y.-X. Jiang, B.-W. Zhang, Y.-R. Cai, S.-G. Sun, High activity of cubic PtRh alloys supported on graphene towards ethanol electrooxidation, Phys. Chem. Chem. Phys. 16 (2014) 13662–13671.
[60] A.N. Geraldes, D.F. da Silva, E.S. Pino, J.C.M. da Silva, R.F.B. de Souza, P. Hammer, E.V. Spinacé, A.O. Neto, M. Linardi, M.C. dos Santos, Ethanol electro-oxidation in an alkaline medium using Pd/C, Au/C and PdAu/C electrocatalysts prepared by electron beam irradiation, Electrochim. Acta 111 (2013) 455–465.